Sea Surface Heights obtained from Modular Ocean Model simulation and comparison with Topex/Poseidon data for the Indian Ocean

P S SWATHI and K S YAJNIK[1]

CSIR Centre for Mathematical Modelling and Computer Simulation (C-MMACS) Bangalore 560 037, India
[1]*Present Address: Regal Manor, 2/1 Bride St, Langford Town, Bangalore 560 025, India*
email: ksy@letterbox. com

The Modular Ocean Model (MOM) is perhaps the most versatile ocean model available today for the simulation of the large scale circulation of the ocean. The Topex/Poseidon altimeter which has been operating since September 1992 has been providing sea surface heights (SSH) of the accuracy of 5–10 cms with a repeat cycle of 10 days. We examine in this paper, the SSH in the Indian Ocean obtained from a global simulation of MOM with a resolution of 1° in the longitude, 1/3° in the latitude between 30°S and 30°N and 20 levels in the vertical with climatological windforcing and restoring conditions on temperature and salinity. They are compared with the SSH from the Topex/Poseidon altimeter after suitable filtering in the time domain to remove smaller time and length scales. In addition, unfiltered data from both sources are analysed by estimating the cross-spectral density to find the coherence and cross-phase at different frequencies. The agreement between the two, over most of the Northern Indian Ocean, especially the Arabian Sea and the Bay of Bengal is quite good.

1. Introduction

The Topex/Poseidon altimeter launched in August 1992 has been hailed as one of the landmark space-borne instruments by the oceanographic community. The altimeter provides the sea-surface height (SSH) with a repeat cycle of 10 days. Improvements in the orbit determination, better sampling of ocean tides and advanced atmospheric corrections have contributed to the vastly improved accuracy of Topex/Poseidon altimeter compared to earlier payloads. However, the accuracy is still limited by the accuracy of the geoid models employed in the interpretation of data. With rapid advances in this area, the accuracy is expected to reach 2 cm in the near future (Cheney *et al* 1994). Many comparisons with tide gauge records (Fu *et al* 1994; G T Mitchum 1994) have shown that an RMS accuracy of 5 cm is possible with current data processing techniques.

The accuracy of the altimeter has spurred the oceanographic community to undertake a variety of investigations with the data. Two special issues of the Journal of Geophysical Research-Oceans (Cheney 1994, 1995) were devoted to several aspects of this investigation ranging from geoid modelling to physical oceanography. For instance, a few studies (Nerem 1995 and Minster *et al* 1995) have tried to use the data to find a direct evidence of global sea level rise. From their studies, it appears that the global mean sea level is rising at a rate of 5 mm/year, though the jury is still out on this issue. Better estimates of this figure are expected to become available with a longer (10 years or so) data set. The first direct observation of Rossby waves has been made by Chelton and Shlax (Chelton and Schlax 1996) with this data. Several dynamical features of ocean currents, notably the Kuroshio extension (Qiu 1995; Hwang 1996) have been investigated.

Keywords. Topex/Poseidon; altimeter; Modular Ocean Model; Indian Ocean; large scale circulation; cross-spectral density.

Proc. Indian Acad. Sci. (Earth Planet. Sci.), **106**, Nos 1 & 2, June 1997, pp. 43–53

There have been a few studies which have compared model results from ocean general circulation models with Topex/Poseidon data. A seminal paper by Stammer and Wunsch (Stammer and Wunsch 1994) compared SSH from the altimeter with those obtained from a global eddy-resolving model of Semtner and Chervin with a 0.25° resolution. They also compared the dynamic heights obtained from the climatological atlas of Levitus (Levitus 1982) and found a good agreement among all the three when annual averages were compared. A careful analysis of the differences between them at a smaller time scale using a spatial spherical harmonic expansion as well as a low order frequency spectrum showed that an accuracy of 5 cm is possible at present. In a more recent work, the same authors (Wunsch and Stammer 1995) have used a two-year record of the data and performed a spectral decomposition both in space and time. They point out that the altimeter data along with other observations will yield improved spatial coherence and better estimates of secular sea level rise. Other model studies include that of Behringer (Behringer 1994) who studied the SSH variations in the Atlantic. The model employed by him is identical to ours (section 2) where he used Hellerman and Rosenstein winds to provide the wind forcing and restoring conditions for heat and salt. However, in contrast to his limited domain model ours is global which avoids problems with open boundaries. While he has used the dynamic height diagnosed from the model as a surrogate, we have solved an additional Poisson equation (section 2) to compute the surface pressure. He found a very good correlation in the amplitude of the annual cycle with an RMS deviation of 5 cm between the altimeter data and model results. Hughes (1995) has performed a similar comparison with the FRAM model in the Southern Ocean in order to study the propagation of Rossby waves. In another study with the FRAM model, Park and Gamberoni (Park and Gamberoni 1995) have found a good agreement in the 18-month averages of altimeter, FRAM and Levitus dynamic height data sets. Chao and Fu (Chao and Fu 1995) have also made a comparison between Topex data and an OGCM for the period 1992–1993 using NMC analysed forcing for winds and heat flux. They have noted that the annual period is well represented in the model while major discrepancies exist in parts in the Pacific and Atlantic for shorter time scales. Also, they have found that the variabilities are apparently barotropic responses to changes in the wind forcing.

The emphasis in the last year has shifted towards the assimilation of Topex/Poseidon data into ocean models. From the pre-Topex work of Mellor & Ezer (Mellor and Ezer 1991), recent publications which focus on data assimilation include Vogeler and Shroeter (Vogeler and Shroeter 1995) and Morrow and Demey (Morrow and Demey 1995) where Geosat and Topex data, respectively, were assimilated into a quasi-geostrophic model. A reduced gravity shallow water model with Kalman filtering for assimilating Topex data has been reported by Fukumori (Fukumori 1995). An assimilation system for the Gulf stream has been developed by Blayo *et al* (1996). In their most recent studies Wunsch and his co-workers have advocated the assimilation of a combination of alimetric, tomographic and hydrographic data into ocean models to improve the accuracy of forecasting (Ganachaud *et al* 1997; Menemenlis *et al* 1997).

Many of the above studies are focused on the Atlantic and the Pacific. In contrast, the Indian Ocean has received only a passing mention in global studies. Recently, Bahulyan and Shaji 1996, have computed SSH from their limited-area diagnostic model of the Indian Ocean (Bahulyan and Shaji 1996) but have not made any comparisons with real data. It is our intention in this paper to make a detailed time and frequency domain analysis of the altimeter data over the Indian Ocean and the outputs from a global simulation for the same area using a contemporary ocean general circulation model.

The Modular Ocean Model (MOM) (Pacanowski 1995; Bryan 1969) is perhaps the most versatile three-dimensional ocean model in existence today. The SSH can be computed from MOM by solving an additional Poisson equation. We provide a brief description of MOM and the steps to extract SSH as a diagnostic in section 2. In section 3 we outline the detailed conditions of the global MOM simulation. In section 4 we make the comparison between MOM and Topex/Poseidon.

2. Modular Ocean Model

We briefly describe the salient features of MOM pertinent to our discussion leaving the reader to refer to MOM Users Guide (Pacanowski 1995) for a more complete discussion. The basic equations for the conservation of momentum are

$$u_t + L(u) - \frac{uv\tan\phi}{a} - fv = -\frac{1}{\rho_0 a\cos\phi}p_\lambda + (\kappa_m u_z)_z + F^u, \quad (1)$$

$$v_t + L(v) + \frac{u^2\tan\phi}{a} + fu = -\frac{1}{\rho_0 a}p_\phi + (\kappa_m v_z)_z + F^v, \quad (2)$$

where u and v are zonal and meridional velocities, respectively, λ is the longitude, ϕ is the latitude, a is the radius of the earth, $f = 2\Omega\sin\phi$ is the coriolis parameter, ρ_0 is the reference density, κ_m is

the vertical eddy viscosity and p is the pressure. The operators L and F are the advection and horizontal friction terms, whose expressions can be found in Pacanowski (1995). Due to vertical stratification, horizontal and vertical diffusion are parameterized differently. The vertical momentum equation is reduced to the hydrostatic equation. In order to suppress the fast moving surface gravity waves, the rigid-lid approximation is employed (i.e. $w = 0$ at $z = 0$). With this assumption it is possible to separate the solution into two modes, the external mode, which is depth independent representing the barotropic flow and the internal mode, which is depth dependent, representing the baroclinic flow.

Equations (1) and (2) are integrated over the ocean depth $H(\lambda, \phi)$ to yield

$$-\left(\frac{\Psi_\phi \cos\phi}{H}\right)_t = -(p_s)_\lambda + \frac{f}{H}\Psi_\lambda + FU\cos\phi, \tag{3}$$

$$\left(\frac{\Psi_\lambda}{H\cos\phi}\right)_t = -(p_s)_\phi + \frac{f}{H}\Psi_\phi + FV, \tag{4}$$

where p_s is the surface pressure and the terms FU and FV are given by

$$FU = -\frac{a}{H}\int_{-H}^{0}\left(L(u) - \frac{uv\tan\phi}{a} - F^u + \frac{g}{a\rho_0\cos\phi}\int_z^0 \rho_\lambda \mathrm{d}\xi\right)\mathrm{d}z, \tag{5}$$

$$FV = -\frac{a}{H}\int_{-H}^{0}\left(L(v) - \frac{u^2\tan\phi}{a} - F^v + \frac{g}{a\rho_0}\int_z^0 \rho_\phi \mathrm{d}\xi\right)\mathrm{d}z, \tag{6}$$

and the stream function Ψ is defined as

$$\Psi_\lambda = a\cos\phi\int_{-H}^{0} v\mathrm{d}z, \tag{7}$$

$$\Psi_\phi = -a\int_{-H}^{0} u\mathrm{d}z. \tag{8}$$

Notice that the pressure p has been decomposed into two terms, i.e., $p = p_s + \int_z^0 \rho\,\mathrm{d}\xi$ using the hydrostatic

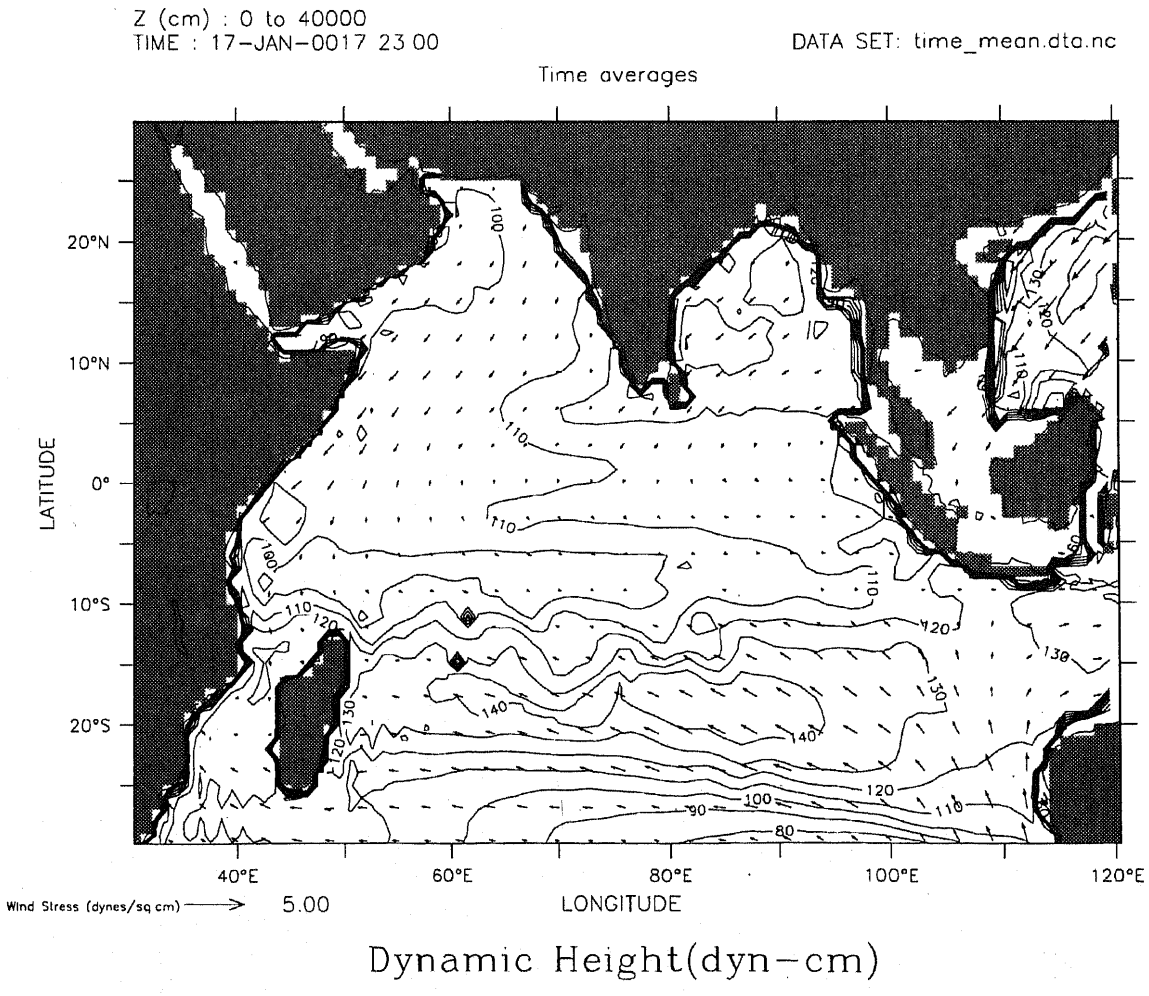

Figure 1. Dynamic height and windstresses over the Indian Ocean in January.

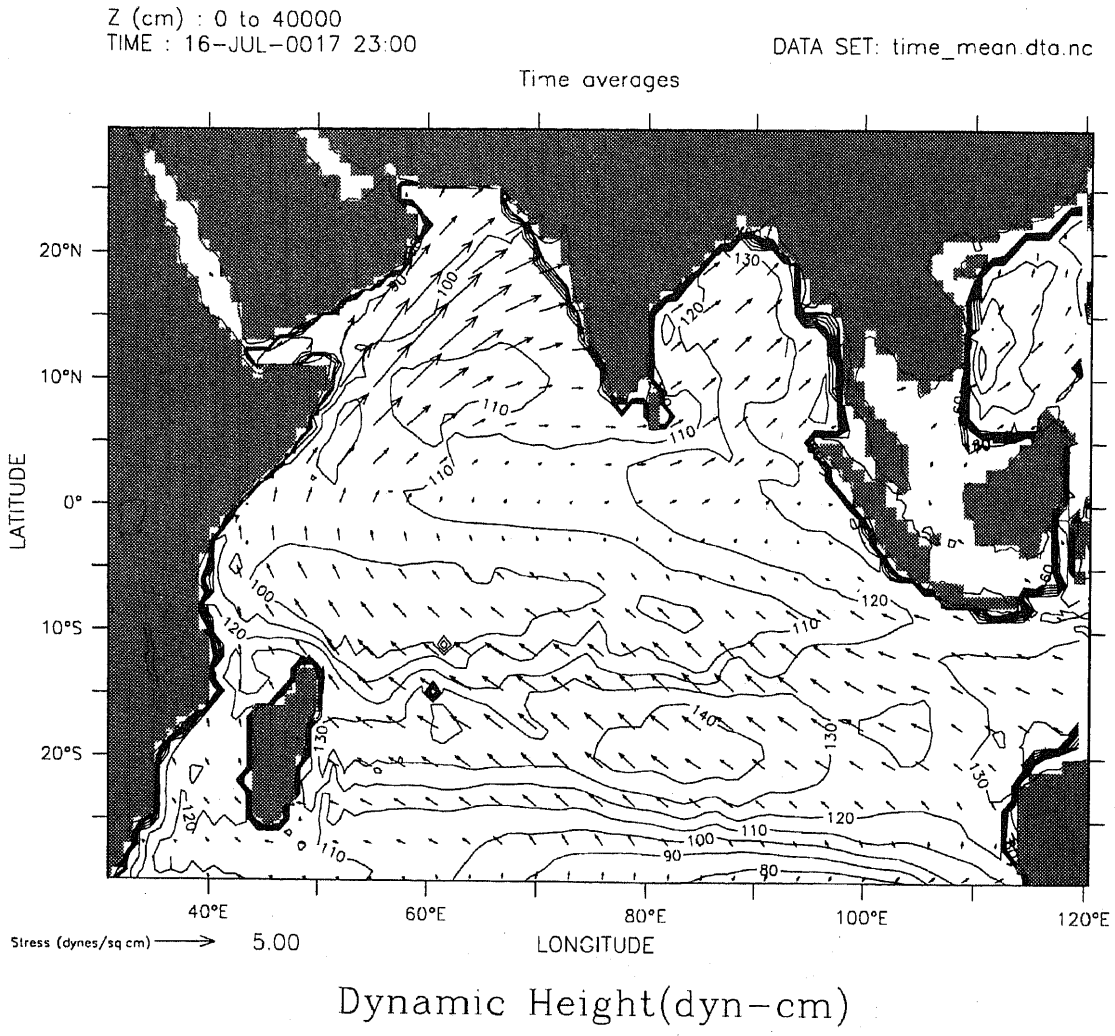

Figure 2. Dynamic height and windstresses over the Indian Ocean in July.

approximation. Elimination of p_s yields:

$$\left(\frac{\Psi_\lambda}{H\cos\phi}\right)_{\lambda t}+\left(\frac{\Psi_\phi\cos\phi}{H}\right)_{\phi t}=FV_\lambda-(FU\cos\phi)_\phi$$
$$-\Psi_\lambda\left(\frac{f}{H}\right)_\phi+\Psi_\phi\left(\frac{f}{H}\right)_\lambda \qquad (9)$$

Equation 9 is solved at every time step in MOM to yield the stream function. To recover the surface pressure, p_s one differentiates equation 3 with respect to λ and equation 4 with respect to ϕ to yield a Poisson equation for p_s as follows:

$$\nabla\bullet H\nabla p_s=X, \qquad (10)$$

where X contains all the terms which can be determined from equations 3 and 4 after differentiation. The sea surface height is determined from p_s by dividing it by $\rho_0 g$. The temperature and salinity fields are computed prognostically by solving additional transport equations. The density field is computed with the UNESCO equation of state (Pond and Pickard 1980).

3. Global ocean simulation with MOM

A horizontal grid (362 × 273) was selected with uniform 1° resolution in the longitude and 1/3° in the latitude between 30°S and 30°N increasing to 2° at the poles. There were 20 levels in the vertical with 10 in the top 100 metres. The bottom topography was interpolated to every grid point from the Scripps data base. There were approximately 2 million grid points with four 3-D prognostic variables (u, v, temperature and salinity) and one 2-D prognostic variable Ψ at each horizontal grid point. The Philander-Pacanowski Richardson number based scheme (Pacanowski and Philander 1981) was implemented for vertical mixing. A constant horizontal mixing scheme with $A_m = 10^7\,\mathrm{cm}^2/\mathrm{s}$ and $A_H = 5\times10^6\,\mathrm{cm}^2/\mathrm{s}$ was used for horizontal mixing. The time step was taken to be 45 minutes to satisfy CFL condition everywhere. The elliptic equations for the stream function and surface pressure were solved with the 9-point conjugate gradient solver.

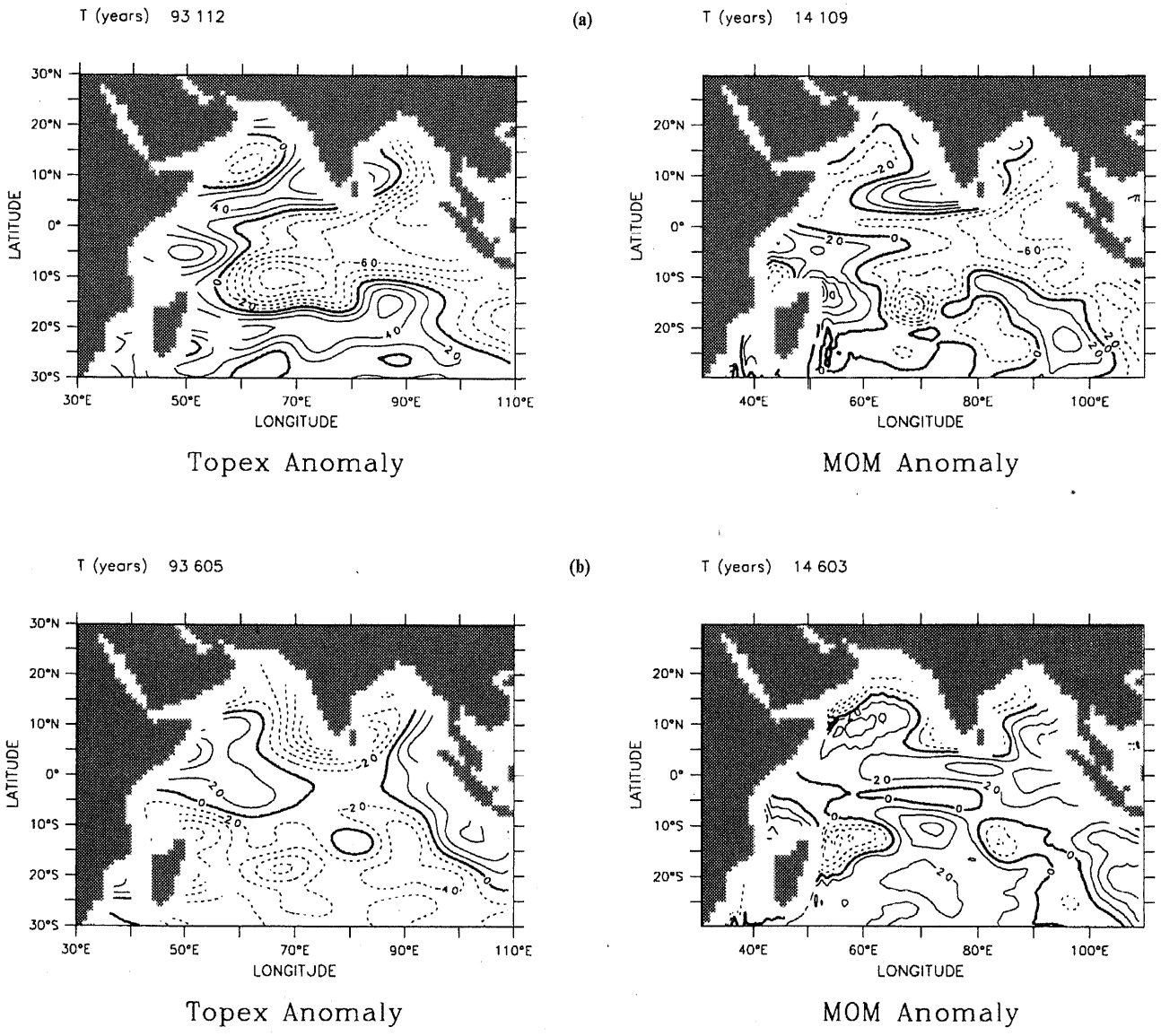

Figure 3. Anomalies of sea surface height (SSH) from Topex/Poseidon data and the global simulation of MOM. The time given at the top left of the Topex Panel are actual times in years. The time in the MOM panel is the simulation time. The interest is in the fractional part of time which has to be synchronized. The MOM simulation is 1 day behind. The top panels (**a**) are for a day in February (NE monsoon season) and the bottom panels (**b**) are for a day in August (SW monsoon). The data have been low-pass filtered according to Chelton and Schlax (Chelton and Schlax 1996).

The model was forced on the surface with monthly-mean climatological windstresses interpolated to each time step (Hellerman and Rosenstein 1983). The time interpolation was based on a linear interpolation between two time-adjacent data sets centred at mid-point of each month. Initial conditions for temperature and salinity were prescribed from the Levitus data base (Levitus 1982) at each grid point. The surface tracers were damped to Levitus values with a restoring time scale of 50 days and depth scale of 10 m (Pacanowski, personal communication). The damping to Levitus was done due to the absence of reliable surface flux data. We realise that this would contribute to errors in the steric heights computed by MOM. However, when we computed heat flux as a diagnostic from MOM, we found that the deviations from climatology were of the order of a few 10's of W/sq.m and may not significantly impact on our results.

In order to synchronize with Topex/Poseidon times, the model output was averaged and generated every 10 days corresponding to Topex's repeat cycle. The model was started from rest and run completely run in double precision (Pacanowski personal communication) to avoid round-off error accumulation. After the initial adjustment period of a few years, the model settled down to a reasonably steady annual pattern for the upper ocean. The results from year 15 of the model run are used in this study.

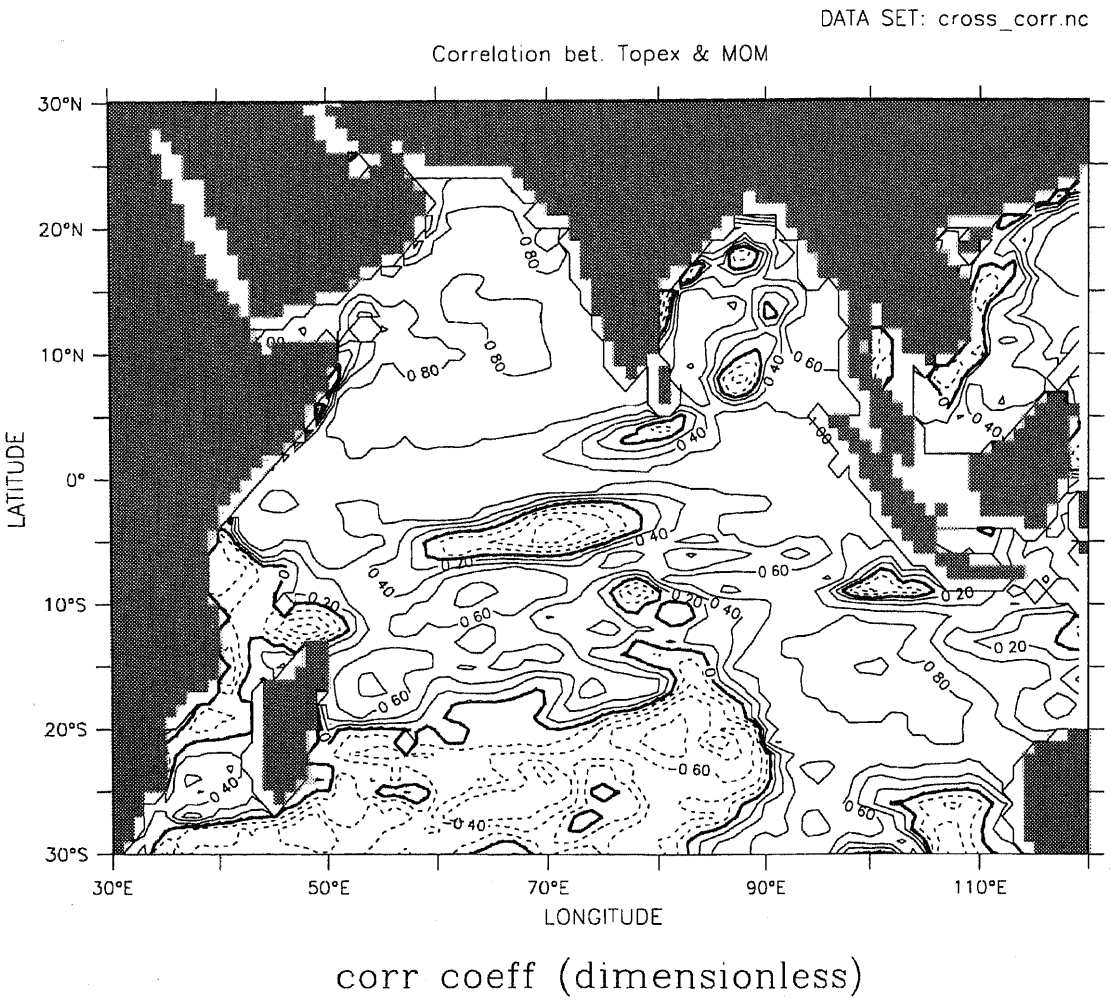

Figure 4. Correlation coefficient between Topex/Poseidon and MOM data. Positive values indicate good correlation while negative ones indicate anti-correlation.

4. Results and Discussion

4.1 *Dynamical Aspects*

The strongest influence on the circulation of the Indian Ocean, including the Arabian Sea and the Bay of Bengal, is the seasonal reversal of the monsoon winds. From the mild NE monsoon winds over the Arabian Sea between December and March (figure 1), winds change to the intense SW monsoon between June and September (figure 2). The resulting change in the circulation is drastic (Hastenrath and Greichar, charts 154–165, 1989). This change and our geographical proximity are our reasons for studying the Indian Ocean region in great detail, even though the results are available for the whole globe from our simulations. During the NE monsoon season, the North Equatorial Current flows westwards and the currents along the African coast are southwards. The South Equatorial counter current flows eastwards and the southern gyre system is present below 5°S throughout the year. During the SW monsoons, the current along the North African coast is directed northwards with speeds as high as 150–200 cm/s along with the presence of a 2-gyre system off the Horn of Africa. The NEC now flows eastwards. All these features are also reproduced in the MOM simulations (not shown here). As this paper deals with sea surface heights, we feel that it would be more apt to compare the dynamic topography between MOM results and climatology (Hastenrath and Greichar 1989) to get a comprehensive view of all the features of the Indian Ocean circulation.

Figures 1 and 2 show the dynamic height computed from MOM simulations for January and July, respectively. These are computed by integrating the specific volume anomaly between the surface and 400 m. They may be compared directly with the geopotential anomaly charts 142 and 148 of Hastenrath and Greichar's Atlas. All the features which are present in the Atlas are also present in MOM simulations although the simulations are consistently 10 dyn-cm higher. Usually it is the spacing between contours which is of interest as it gives an indication of the magnitude of the geostrophic flow between them. In January, we notice (figure 1) that the ridge

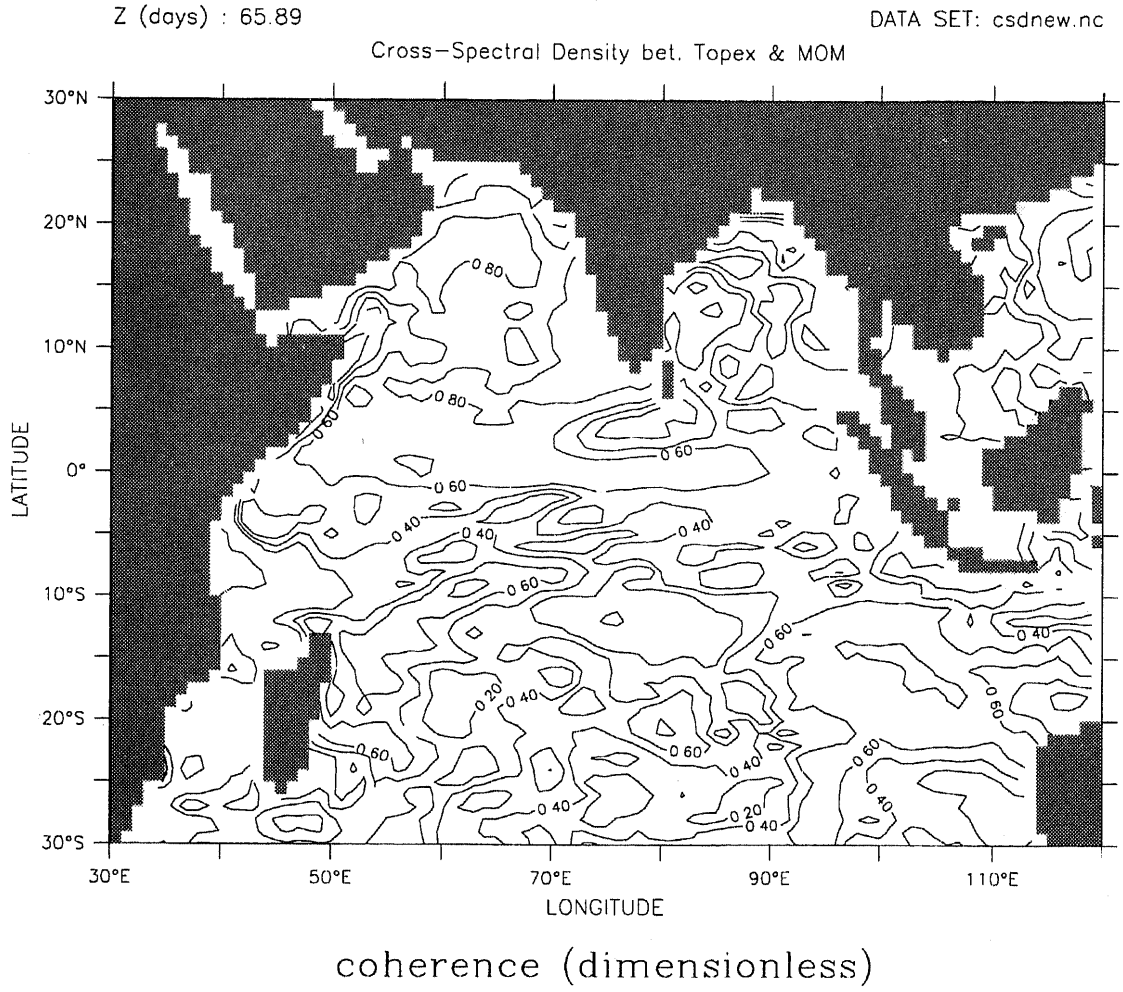

Figure 5. Coherence between Topex and MOM data sets from cross-spectral density estimation for a period of 65.89 days. Input data to the cross-spectral estimation are unfiltered anomalies.

in the southern Indian Ocean is oriented in the east-west direction, while the chart 142 indicates a small tilt upwards towards the east. The highs in the Indonesian throughflow region, the south China Sea and the Bay of Bengal are also found in both data sets. The lows off Africa near the equator are also present. Also, notice the absence of strong currents (close isolines) near the Horn of Africa. During the SW monsoon (figure 2), there is a dramatic change off the Horn of Africa by the presence of close contours, indicating a large flow in that region. The ridge in the southern Indian Ocean is less pronounced with the peak shifting eastwards. All these features are consistent with chart 148 of the Atlas.

4.2 *Comparison between MOM and Topex Data*

4.2.1 *Time Domain*

A direct comparison of the sea surface heights (SSH) between the two data sets is precluded due to the following reasons: 1) the two data sets are referenced to different datums (geoid in the case of Topex and global zero mean level in case of MOM), and 2) the presence of high frequency variability in the Topex data, both in space and time and its absence in MOM. Both the above problems are handled by studying the anomalies of SSH instead of absolute heights. In both cases we subtract the annual mean at each spatial location from the data. In addition, for addressing the second problem, we employ low-pass filtering as done by Chelton and Schlax (Chelton and Schlax 1996). The low-pass filtering is applied only for time domain comparisons and the data are not filtered for frequency domain analysis done in section 4.2.2. The intention of doing time domain analysis is only to show that the magnitude of the anomalies are comparable.

In all the subsequent analysis, we use Topex data from the year 1993 at $1^\circ \times 1^\circ$ spatial resolution at 10 day intervals. The MOM simulation results are time averages over a 10-day period coincident in time (Julian days) with Topex data. The results of the 15th year of MOM simulation are used in the analysis.

Figure 3(a) shows a comparison between the two data sets during the NE monsoon. Although we tried to synchronize MOM times with Topex

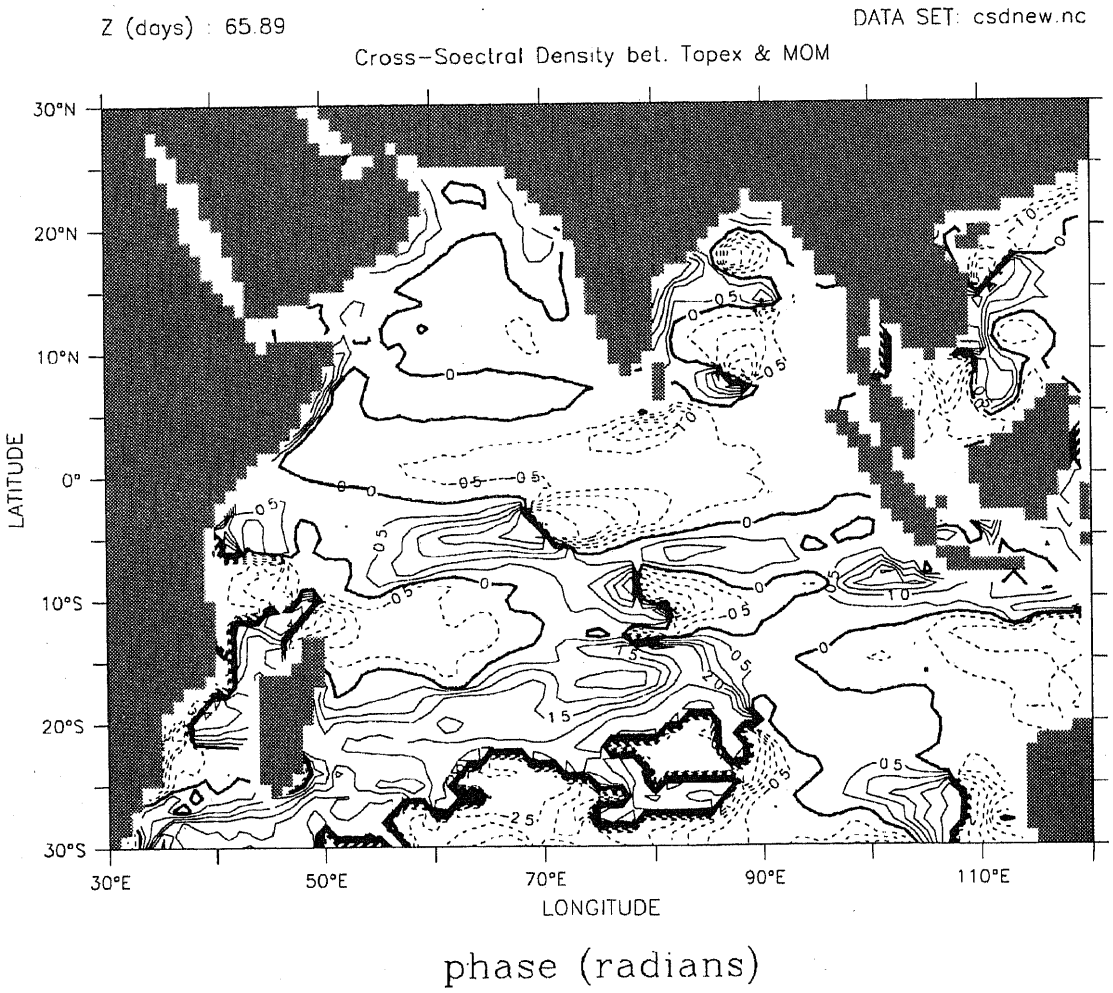

Figure 6. Cross-phase between Topex and MOM data sets from cross-spectral density estimation for a period of 65.89 days. A value of 0 indicates that both signals are in phase.

times, we were off by 1 day. This can be seen in the 0.003 difference in the fractional part of time in years shown at the top of each frame. The contour interval in all the plots is 2 cm with negative values shown in broken lines. The SSH anomaly around the Indian coast in February (figure 3a) shows a positive anomaly which is comparable in both data. The positive SSH anomaly in February around the south Indian peninsula captured by the MOM simulation agrees well with altimeter data. The negative anomaly off the Somali and Arabian coast is also captured although it tends to be slightly lower in the MOM results. The negative anomaly over most of the Bay of Bengal is also comparable. The deep low off 60°E, 10°S is also captured in MOM though it tends to be shifted slightly south. The signals from the Pacific are also comparable. During August (figure 3b) the anomalies around the Indian, the Arabian and the Somali coasts are predominantly negative and have been reproduced well by MOM. Also notice the positive anomaly which is propagating from the Pacific into the Indian Ocean. There are however qualitative and quantitative differences in the Southern Ocean and these are reflected clearly in the frequency domain analysis of the next section.

4.2.2 *Frequency Domain*

As mentioned in the last section, we use unfiltered anomalies to study the cross-correlation between the two data sets at different frequencies. The standard cross-correlation coefficient (at zero lag) is shown in figure 4. Notice the high correlation (> 0.8) between the two in the Arabian Sea, parts of the north Indian Ocean and the Indonesian throughflow region. Negative correlations exist in small parts of the Bay of Bengal, the Equatorial Indian Ocean between 60°E and 80°E, 0°S and 5°S, the Mozambique region and the southern Indian Ocean. We attribute the negative correlations predominantly to smoothed forcing in MOM and perhaps incomplete physics. However, it is encouraging to see that the entire northern Indian Ocean except parts of Bay of Bengal are well correlated.

Next we perform a cross-spectral density analysis to find the linear correlation between the two

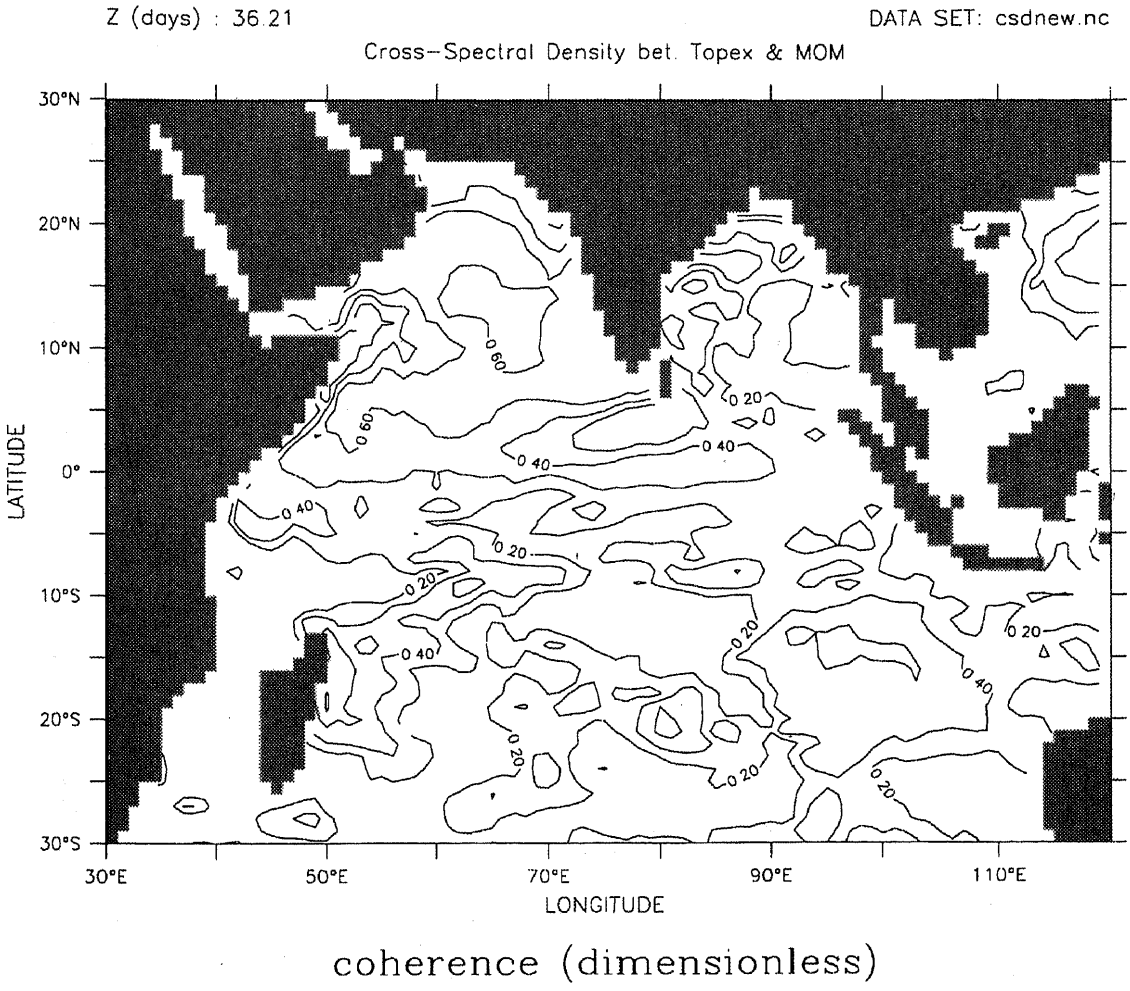

Figure 7. Coherence between Topex and MOM data sets from cross-spectral density estimation for a period of 36.21 days.

data sets (x and y, which stand for Topex and MOM) at different frequencies. The Nyquist frequency of both the data sets is $1/(2 \times 10)$ days^{-1} and we may resolve frequencies lower than this. However, we do not expect high frequencies close to Nyquist to be well correlated due to the smooth forcing of MOM.

The methodology employed to find the cross-spectral density (Hearn and Metcalfe 1995) is as follows. The smoothed cross-spectral density estimate of two series, x and y is given by

$$\Gamma_{xy}(\omega) = \sum_{k=(N-1)}^{N-1} W(k)\Upsilon_{xy}(k)e^{-i\omega k}, \tag{11}$$

where $W(k)$ is a set of weights (Parzen window with $M = 4$, in our case, Hearn and Metcalfe 1995), $\Upsilon_{xy}(k)$ is the cross-covariance at lag k. The real and imaginary parts of $\Gamma_{xy}(\omega)$ can be written as

$$\Gamma_{xy}(\omega) = \mathrm{co}(\omega) + \mathrm{iquad}(\omega), \tag{12}$$

where co is the co-spectrum and the quad is the quadrature spectrum. The coherence between the two signals is given by

$$\mathrm{coherence}(\omega) = \frac{|\Gamma_{xy}|}{\sqrt{\Gamma_{xx}\Gamma_{yy}}}. \tag{13}$$

Coherence corresponds to the cross-correlation coefficient between x and y at frequency ω. By definition, coherence always lies in the (0,1) interval with 0 indicating no correlation and 1 indicating perfect correlation. The cross-phase between x and y is given by

$$\mathrm{phase}(\omega) = \mathrm{atan}\left(\frac{\mathrm{quad}(\omega)}{\mathrm{co}(\omega)}\right). \tag{14}$$

The phase indicates how much one signal is leading (or lagging) the other. Although cross-spectral density estimation is made for a set of frequencies between 0 and Nyquist, we only show results for two representative frequencies (periods = 66 and 36 days).

Figure 5 shows the coherence between Topex and MOM at a period of 65.89 days. The coherence is high (> 0.8) over most of the Arabian Sea. The southern Indian Ocean shows lower correlation as is to be expected from the earlier analysis. From the cross-phase shown in figure 6, we notice that the two signals are in-phase over most of the Arabian Sea while they are out-of-phase in several parts of the southern

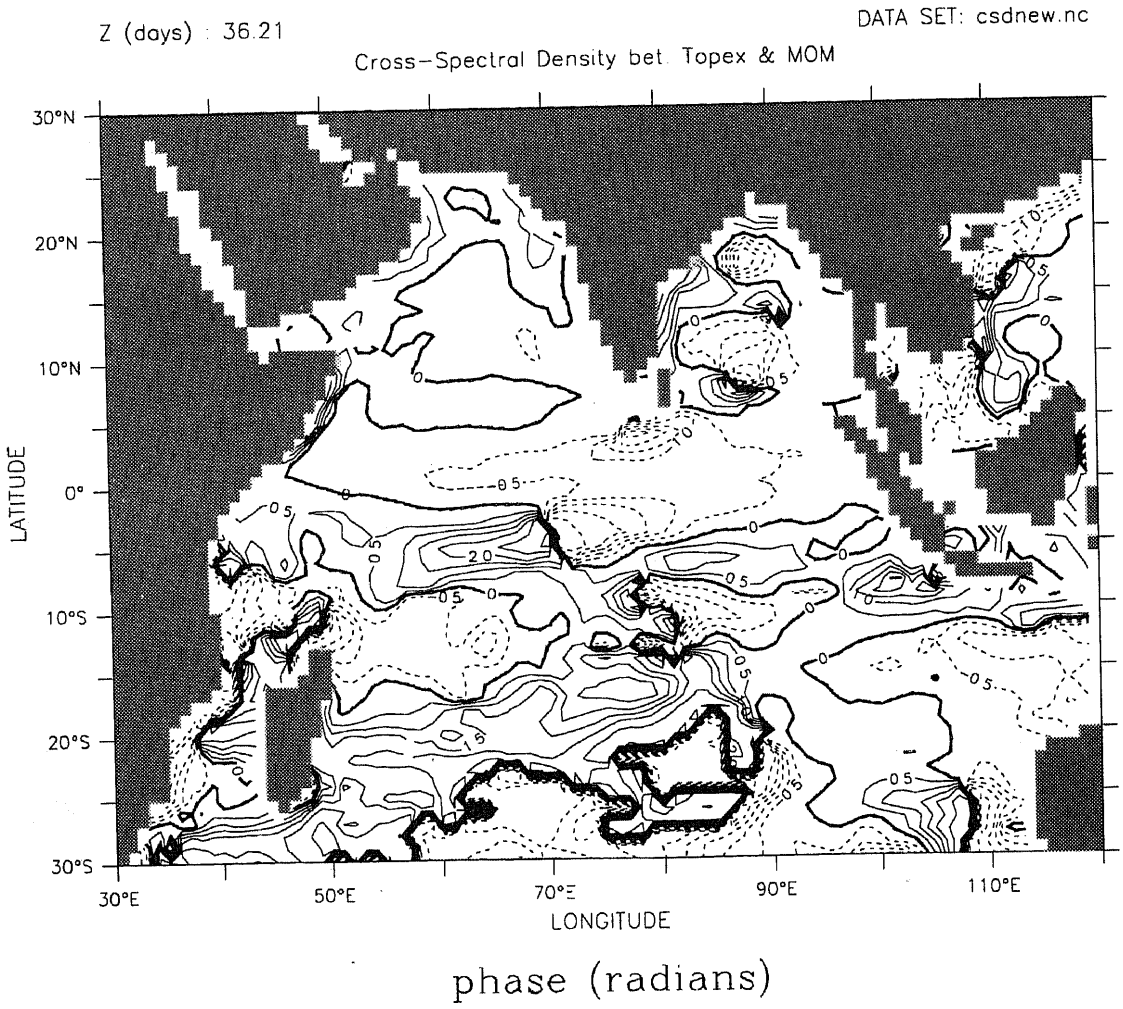

Figure 8. Cross-phase between Topex and MOM data sets from cross-spectral density estimation for a period of 36.21 days.

Indian Ocean and the Bay of Bengal. The coherence at 36.21 days period (figure 7) shows a reduction in the cross-correlation in all the areas compared to figure 5. This has to be expected as we are much closer to Nyquist in this case. The phase (figure 8) is almost a replica of the phase at 66 days period (figure 6). The results for all other frequencies (not shown here) can be surmised from figures 5 and 7. For periods greater than 66 days, the coherence continues to increase at a small rate, while for periods less than 36 days (until 20 days), coherence progressively decreases.

5. Conclusions

We have shown that a good agreement exists between the anomalies of SSH seen by Topex/Poseidon and those computed by MOM over a typical year, both quantitatively as well as qualitatively. The correlation between the two in the northern Indian Ocean, especially in the Arabian Sea is better than in the southern Indian Ocean. Cross-spectral density estimates between the two show that the coherence between the two signals at low frequency is quite high and the signals are in phase over most of the Arabian Sea even when MOM is forced with climatology. Extension of this work to actual forcing with satellite and *in situ* winds, and air-sea fluxes is expected to improve the correlation over all space and time scales.

Acknowledgements

We gratefully acknowledge the help of Ron Pacanowski, GFDL for his active involvement in the study; John Sheldon, GFDL for his higher level netCDF modules which helped enormously in processing the MOM output; Steve Emmerson and Russ Rew at Unidata, NCAR for providing netCDF libraries and porting assistance; and Jim Davison, PMEL for providing Ferret for visual analysis of data. The Topex/Poseidon data were obtained from the Centre for Space Research, University of Texas. We also wish to thank R P Thangavelu, C-MMACS for his assistance in porting several packages to Convex and workstations. Finally, the authors are deeply grateful to the Department of Ocean Development for supporting this work under the MARSIS programme.

7. List of Symbols

λ	Longitude.
ϕ	Latitude.
u	Zonal velocity.
v	Meridional velocity.
$L(u)$	Advective operator.
f	Coriolis parameter.
ρ_0	Reference density.
a	Radius of the earth.
p	Pressure.
κ_m	Vertical eddy viscosity.
F^u	Horizontal friction terms in equation 1.
F^v	Horizontal friction terms in equation 2.
Ψ	Stream function.
H	Ocean depth.
p_s	Surface pressure.
FU	Vertical Integrals defined in equation 5.
FV	Vertical Integral defined in equation 6.
$\Gamma_{xy}(\omega)$	Cross-spectral density estimate defined in equation 11.
$W(k)$	Set of weights in equation 11.
$\Upsilon_{xy}(k)$	Cross-covariance at lag k.

References

Bahulyan N and Shaji C 1996 Diagnostic Model of 3-D circulation in the Arabian Sea and Western Equatorial Indian Ocean: Results of monthly mean sea surface topography; Accepted for publication in INSA, Physical Sciences, Part A

Behringer D W 1994 Sea surface height variations in the Atlantic Ocean: A comparison of Topex altimeter data with results from an ocean data assimilating system. 99 (C12); *J. Geophys. Res.-Oceans* 24685–24690

Blayo E, Verron J, Molines J M and Testard L 1996 Monitoring of the Gulf Stream path using Geosat and Topex/Poseidon altimetric data assimilated into a model of ocean circulation; *J. Marine Systems* **8** 73–89

Bryan K 1969 A numerical method for the study of the circulation of the world ocean; *J. Comp. Phys.* **4** 347–376

Chelton D B and Schlax M G 1996 Global Observations of Oceanic Rossby Waves; *Science* **272** 234–238

Cheney R E, Miller L, Agreen R, Doyle N and Lillibridge J 1994 Topex/Poseidon: The 2-cm solution; *J. Geophys. Res.-Oceans* **99** 24553–24563

Cheney R E 1995 Special Section: Topex/Poseidon. Scientific Results, Preface; *J. Geophys. Res.-Oceans* **100** 24893

Chao Y and Fu L L 1995 A comparison between Topex/ Poseidon data and a global ocean general circulation model during 1992–93; *J. Geophys. Res.-Oceans* **100** 24965–24976

Fu L L, Christiansen E J, Yamarone C A, Lefebvre M, Menard Y, Dorrer M and Escudier P 1994 Topex/Poseidon: Mission overview; *J. Geophys. Res.-Oceans* **99** 24369–24382

Fukumori I 1995 Assimilation of Topex sea level measurements with a reduced gravity, shallow water model of the tropical Pacific Oceans; *J. Geophys. Res.-Oceans* **100** 25027–25043

Ganachaud A, Wunsch C, Kim M C and Tapely B 1997 Combination of Topex/Poseidon data with a hydrodynamic inversion for determination of ocean general circulation and its relation to geoid accuracy; *Geophys. J. Inter.* **128** 708–722

Hastenrath S and Greichar L L 1989 Climatic Atlas of the Indian Ocean, Part III: Upper-Ocean Structure (The Univ. of Wisconsin Press)

Hearn G E and Metcalfe A V 1995 Spectral Analysis in Engineering, Concepts and Cases, (London: Arnold Publications)

Hellerman P J and Rosenstein M 1983 Normal monthly wind stresses over the world ocean with error estimtes; *J. Phys. Oceanography* **13** 1093–1104

Hughes C W 1995 Rossby waves in the Southern Ocean: A comparison of Topex/Poseidon altimetry with model prediction; *J. Geophys. Res.-Oceans* **100** 15933–15950

Hwang C W 1996 A study of the Kuroshios seasonal variabilities using an altimetric gravimetric geoid and Topex/Poseidon altimeter data; *J. Geophys. Res.-Oceans* **101** 6313–6335

Levitus S 1982 Climatological atlas to the world ocean, NOAA Prof. Papers, 13, Department of Commerce

Mellor G L and Ezer T 1991 A Gulf-stream model and an altimetry assimilation scheme; *J. Geophys. Res.-Oceans* **96** 8779–8795

Menemenlis D, Webb T, Wunsch C, Send U and Hill C 1997 Basin scale ocean circulation from combined altimetric, tomographic and model data; *Nature* **385** 618–621

Minster J F, Brissier C and Rogel P 1995 Variations of mean sea level from Topex/Poseidon data; *J. Geophys. Res.-Oceans* **100** 25153–25161

Mitchum G T 1994 Comparison of Topex sea surface heights and tide gauge levels; *J. Geophys. Res.-Oceans* **99** 24541–24543

Morrow R and Demey P 1995 The adjoint assimilation of altimetric, surface drifter and hydrographic data in a quasi-geostrophic model of the Azores Current; *J. Phys. Oceanography* **100** 25007–25025

Nerem R S 1995 Measuring global mean sea level variations with Topex/Poseidon data; *J. Geophys. Res.* **100** 25138–25151

Pacanowski R C 1995 MOM 2 Documentation, User's Guide and Reference Manual, Ver1.0, GFDL Ocean Tech. Report #3, Sept.

Pacanowski R C and Philander G 1981 Parameterization of Vertical Mixing in Numerical Models of the Tropical Ocean; *J. Phys. Oceanography* **11** 1142–1451

Park Y H and Gamberoni L 1995 Large-scale circulation and its variability in the south Indian Ocean from Topex/Poseidon altimetry; *J. Geophys. Res.-Oceans* **100** 24911–24929

Pond S and Pickard G L 1995 Introductory Dynamical Oceanography, 2nd Edition, (Oxford: Butterworths and Heineman)

Qiu B 1995 Variability and Energetics of the Kuroshio Extension and its Recirculation Gyre from the first two year TOPEX data; *J. Phys. Oceanography* **25** 1827–1842

Stammer D and Wunsch C 1994 Preliminary assessment of the accuracy and precision of Topex/Poseidon altimeter data with respect to the large scale circulation; *J. Geophy. Res.-Oceans* **99** 24584–24604

Vogeler A and Schroeter J 1995 Assimilation of satellite altimeter data into an open ocean model; *J. Geophys. Res.-Oceans* **100** 15951–15963

Wunsch C and Stammer D 1995 The global frequency and wavenumber spectrum of oceanic variability estimated from Topex/Poseidon altimetric measurements; *J. Geophys. Res.-Oceans* **100** 24895–24910

MS received 25 October 1996; revised 20 May 1997